RESEARCH ARTICLE | JULY 05 2023

Electron mobility enhancement in *n*-GaN under Ohmic-metal

Kazuya Uryu ; Yuchen Deng ; Son Phuong Le ; Toshi-kazu Suzuki

AIP Advances 13, 075002 (2023)
https://doi.org/10.1063/5.0147137

Electron mobility enhancement in *n*-GaN under Ohmic-metal

Cite as: AIP Advances 13, 075002 (2023); doi: 10.1063/5.0147137
Submitted: 21 March 2023 • Accepted: 7 June 2023 •
Published Online: 5 July 2023

Kazuya Uryu,[1,2] Yuchen Deng,[1] Son Phuong Le,[3] and Toshi-kazu Suzuki[1,a)]

AFFILIATIONS

[1] Center for Nano Materials and Technology, Japan Advanced Institute of Science and Technology (JAIST), 1-1 Asahidai, Nomi, Ishikawa 923-1292, Japan
[2] Advantest Laboratories Ltd., 48-2 Matsubara, Kami-Ayashi, Aoba-ku, Sendai, Miyagi 989-3124, Japan
[3] Department of Physics, Chemistry and Biology (IFM), Linköping University, 581-83 Linköping, Sweden

[a)] **Author to whom correspondence should be addressed:** tosikazu@jaist.ac.jp

ABSTRACT

We investigated the electron transport properties of n-GaN under an Ohmic-metal. Hall measurement results were compared for *n*-GaN (A) before Ti-based metal deposition, (B) after Ti-based metal deposition but before annealing, (C) after Ohmic annealing, and (D) after Ohmic-metal removal, where multi-probe-Hall device measurements are required for (C), while the others, (A), (B), and (D), can be characterized by conventional Hall device measurements. The multi-probe-Hall device measurements for (C) elucidated that, under the Ohmic-metal, the electron concentration is increased and the electron mobility is enhanced in comparison with those for the other cases, (A), (B), and (D). The increased electron concentration indicates that high-density doping takes place in the *n*-GaN by the Ohmic annealing. However, the high-density doping is not observed after the Ohmic-metal removal. Moreover, the electron mobility enhancement under the Ohmic-metal cannot be explained by donor doping with ionized impurity scattering. These suggest that, under the Ohmic-metal, high-density donors are not formed, and high-density polarization doping owing to strain from the Ohmic-metal takes place. From theoretical calculations, we clarified that the increase in the electron density by polarization doping without donors leads to the suppression of ionized impurity scattering and consequently the electron mobility enhancement.

In general, Ohmic contacts are not formed by only metal deposition on semiconductors but formed by subsequent annealing, suggesting that high-density doping takes place in the semiconductors under Ohmic-metals. Due to the high-density doping, the semiconductor electrical properties under the Ohmic-metals are modified from those before Ohmic-metal formation.[1,2] In order to measure the sheet resistance ρ_s under the Ohmic-metals, the end contact resistance method[3–13] and the floating contact resistance method[14–16] have been developed, while the carrier concentration and mobility cannot be evaluated by these methods. Previously, by using multi-probe-Hall devices, we proposed a characterization method for the carrier concentration and mobility under an Ohmic-metal.[17] Applying the method to AlGaN/GaN heterostructures under Ohmic-metals, it is suggested that polarization doping[18] owing to strain from the Ohmic-metal plays a significant role in the formation of Ohmic contact to the AlGaN/GaN heterostructures.[17,19]

In this work, using multi-probe-Hall devices, we investigated the electron transport properties of *n*-GaN under an Ohmic-metal obtained by low-temperature annealing. Recently, in order to reduce the thermal budget, and to suppress rough surface morphology and poor edge acuity of Ohmic-metals,[20] low-temperature annealing around 600 °C[21–25] is preferably employed for Ohmic contacts to *n*-GaN instead of high-temperature annealing at ≥ 800 °C.[26–33] We compared Hall measurement results for *n*-GaN (A) before Ti-based metal deposition, (B) after Ti-based metal deposition but before annealing, (C) after Ohmic annealing, and (D) after Ohmic-metal removal, where multi-probe-Hall device measurements are required for (C), while the others, (A), (B), and (D), can be characterized by conventional Hall device measurements. From the multi-probe-Hall device measurements for (C), we find that the sheet electron concentration n_s is increased and the electron mobility μ_s is enhanced under the Ohmic-metal in comparison with those for the other cases, (A), (B), and (D). This indicates that

high-density doping takes place in the *n*-GaN by the Ohmic annealing but vanishes after the Ohmic-metal removal. Moreover, the electron mobility enhancement under the Ohmic-metal cannot be explained by donor doping with ionized impurity scattering. Thus, we can conclude that high-density donors, such as nitrogen vacancies,[30,34–36] are not formed under the Ohmic-metal. Polarization doping owing to strain from the Ohmic-metal can explain the above results; theoretical calculations show that the increase in the electron density by polarization doping not associated with donors leads to the suppression of ionized impurity scattering and consequently the electron mobility enhancement.

Using an *n*-GaN (27 nm, Si-doped)/GaN (1000 nm) epitaxial structure grown by hot-wall metal-organic chemical vapor deposition[37] on SiC (0001), Hall measurements were carried out for *n*-GaN (A) before Ti-based metal deposition, (B) after Ti-based metal deposition but before annealing, (C) after Ohmic annealing, and (D) after Ohmic-metal removal (Fig. 1). The effective donor doping density in the *n*-GaN is $N_{dd} = N_d - N_a \simeq 4.0 \times 10^{18}$ cm^{-3}, where N_d and N_a are the donor and acceptor densities, respectively. The properties for (A), (B), and (D) can be characterized by conventional Hall device measurements because Ohmic contacts are not formed even for (B). On the other hand, in the case of (C), due to the formation of Ohmic contacts, it is necessary to employ multi-probe Hall devices.[17,19] Below (C) in Fig. 1, we show the schematic top view of the multi-probe-Hall devices with the transmission line model, where an $L \times W$ size Ohmic-metal is formed on the channel. The devices have the current injection electrodes and the multiple voltage probe electrodes, which enable us to measure the lateral voltage V_L and the Hall voltage V_H as functions of the position x with respect to the center of the Ohmic-metal.

The results of the Hall measurements are summarized in Fig. 2. For (A), we obtained a sheet resistance $\rho_s \simeq 5700\ \Omega/\square$, a sheet electron concentration $n_s \simeq 4.4 \times 10^{12}$ cm^{-2}, and the electron mobility $\mu_s \simeq 250$ cm^2/V-s, as plotted by the black point in Fig. 2. This result can be explained by an effective surface barrier height $\Phi_B \simeq 0.85$ eV. In the case of (B), a Ti/Al/Ti/Au metal without annealing is formed, and we obtained $\rho_s \simeq 4600\ \Omega/\square$, $n_s \simeq 5.7 \times 10^{12}$ cm^{-2}, and $\mu_s \simeq 240$ cm^2/V-s, as plotted by the green point in Fig. 2. The increase in n_s by the formation of the Ti/Al/Ti/Au metal is attributed to a decrease in Φ_B from 0.85 to 0.55 eV. In the case of (C), Ohmic annealing at 575 °C in N_2 ambient for 5 min leads to a contact resistance $R_c \simeq 1.5\ \Omega$mm. The multi-probe-Hall devices shown in Fig. 1 have an Ohmic-metal length $L = 200\ \mu$m and widths $W = 1.7, 4.6, 9.7, 20\ \mu$m. Applying current density J_0 (mA/mm) through the current injection electrodes (made of the Ohmic-metal), we measured V_L under no magnetic field $B = 0$ and V_H under a magnetic field $B = 0.32$ T using the multiple voltage probe electrodes (made of the Ohmic-metal). Figure 3 shows the measured V_L/J_0 and $V_H/(J_0 W)$ as functions of the position x for (C). According to the transmission line model, solving the differential equations in Ref. 17, we obtain

$$\frac{V_L(x)}{J_0} = -\frac{\rho_s}{\rho_s + \rho_m}\left(\rho_m x + \rho_s \frac{\sinh(x/L_T)}{L_T \cosh(L/2L_T)}\right), \quad (1)$$

where ρ_m is the metal sheet resistance, ρ_c is the specific contact resistivity, and $L_T = \sqrt{\rho_c/(\rho_s + \rho_m)}$ is the transfer length. The measured results of $V_L(x)/J_0$ are independent of W and can be well fitted

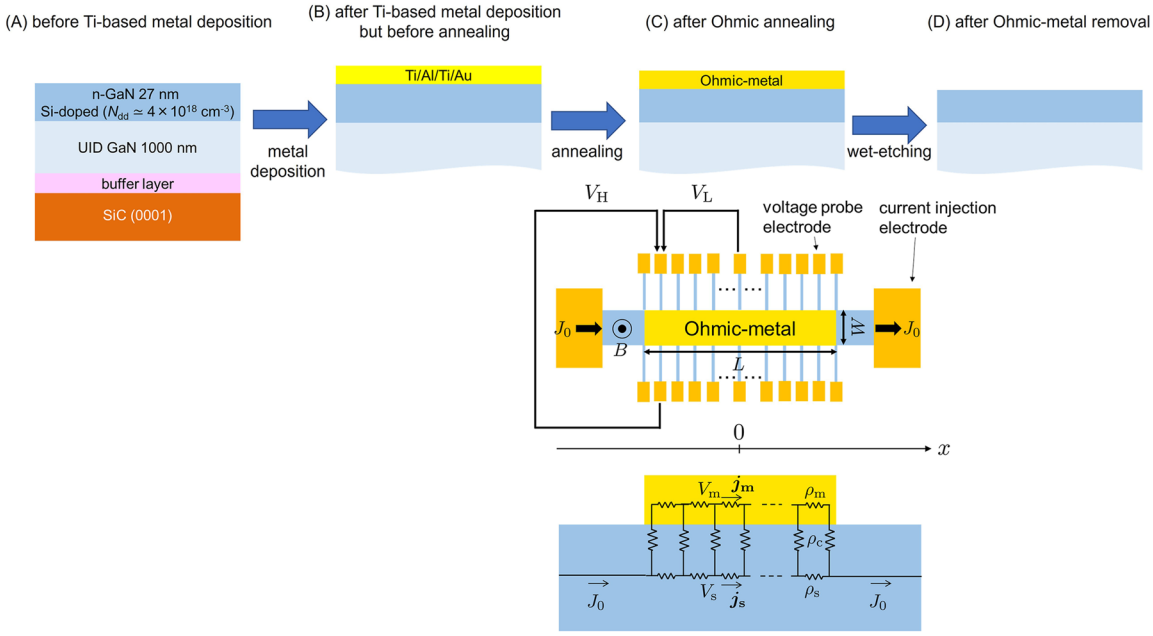

FIG. 1. The schematic cross section for *n*-GaN (A) before Ti-based metal deposition, (B) after Ti-based metal deposition but before annealing, (C) after Ohmic annealing, and (D) after Ohmic-metal removal. Below (C): the schematic top view of multi-probe-Hall devices with the transmission line model.

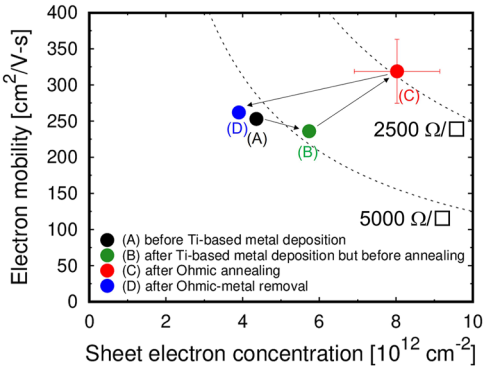

FIG. 2. The relationship between the sheet electron concentration n_s and the electron mobility μ_s for (A)–(D). The dashed-curves show the sheet resistance ρ_s = 2500 and 5000 Ω/□.

by Eq. (1). The fitting gives $\rho_s \simeq (2400 \pm 340)\ \Omega/\square$, $\rho_c \simeq (9.1 \pm 2.8) \times 10^{-6}\ \Omega\text{cm}^2$, $\rho_m \simeq (1.2 \pm 0.1)\ \Omega/\square$, and $L_T \simeq (0.6 \pm 0.08)\ \mu$m. Moreover, from $V_H(x)$ around $x = 0$, we obtain the measured mobility

$$\mu_{\text{meas}} = \frac{1}{BW}\left.\frac{V_H}{\partial V_L/\partial x}\right|_{x=0} \simeq \mu_s - \frac{\rho_s(\mu_s - \mu_m)}{\rho_s + \rho_m}\left(1 - \frac{\tanh(W/2L_T)}{W/2L_T}\right), \quad (2)$$

where μ_{meas} is approximately μ_s for the small-W limit. However, in this case, due to the very small L_T compared with W, the approximation is not valid. In the inset of Fig. 3 (right), we plotted μ_{meas} depending on W and fitted using (2), leading to $\mu_s \simeq (320 \pm 40)\ \text{cm}^2/\text{V-s}$ and $n_s = 1/q\rho_s\mu_s \simeq (8.0 \pm 1.1) \times 10^{12}\ \text{cm}^{-2}$. The obtained results are also shown by the red point in Fig. 2, where the error bars show the three-sigma asymptotic standard errors in the fittings. Under the Ohmic-metal, n_s is increased and μ_s is enhanced in comparison with those for (A) and (B). The increased n_s indicates that high-density doping takes place in the n-GaN by the Ohmic annealing. However, the μ_s enhancement under the Ohmic-metal cannot be explained by donor doping with ionized impurity scattering. In the case of (D), the Ohmic-metal is removed by wet-etching using $H_2O_2 : H_2SO_4$ (1 : 9) and HF. We obtained $\rho_s \simeq 6100\ \Omega/\square$, $n_s \simeq 3.9 \times 10^{12}\ \text{cm}^{-2}$, and $\mu_s \simeq 260\ \text{cm}^2/\text{V-s}$ for (D), as plotted by the blue point in Fig. 2; n_s is even smaller than that for (A). This indicates that high-density donors do not exist after the Ohmic-metal removal. The smaller n_s than that for (A) is due to a slight decrease in the n-GaN thickness after the Ohmic-metal removal as shown below.

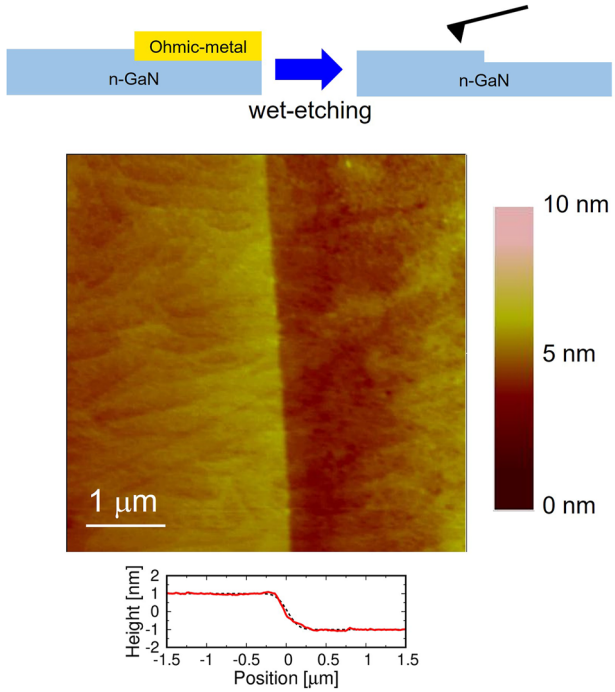

FIG. 4. AFM measurements for (D): an AFM image after the Ohmic-metal removal and the cross-sectional profile.

The decrease in the n-GaN thickness for (D) was measured by atomic force microscope (AFM) as shown in Fig. 4. From the cross-sectional profile, we find that the n-GaN thickness is reduced by

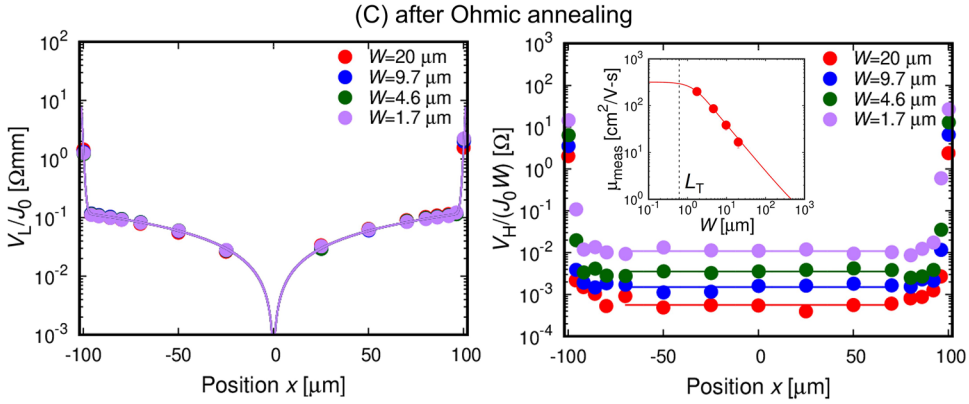

FIG. 3. The measured $V_L(x)/J_0$ (left) and $V_H(x)/(J_0W)$ (right) for (C), with the fitting curves. The inset of the right: the Ohmic-metal width W dependence of the measured mobility μ_{meas}.

≃ 2 nm after the Ohmic-metal removal. This is the cause of the decrease in n_s for (D) and suggests that during the Ohmic annealing, the Ti-based metal reacted with a part of the *n*-GaN to form a metal-like altered layer, such as TiN or GaTiN,[38–40] which was removed by the wet-etching. Furthermore, we fabricated Ni/Au Schottky diodes on the *n*-GaN for (A) and (D) according to the process flow shown in Fig. 5 (left) and obtained the capacitance-voltage characteristics at 1 MHz shown in Fig. 5 (right). We find that the threshold voltage after the Ohmic-metal removal positively shifts due to the decrease in the *n*-GaN thickness. However, around $V_G = 0$, the characteristics of both Schottky diodes well coincide, with the same doping density of $\simeq 4.0 \times 10^{18}$ cm^{-3} for (A) and (D), confirming that high-density donors do not exist after the Ohmic-metal removal. This suggests that high-density donors are not formed under the Ohmic-metal. We consider that the high-density doping under the Ohmic-metal without high-density donors can be attributed to polarization doping[18,41,42] owing to strain from the Ohmic-metal.

In order to estimate the doping density N_D (cm^{-3}) in the *n*-GaN just under the Ohmic-metal, we characterized the temperature dependence of ρ_c for (C). From $V_L(x)/J_0$ measurements for temperature $T = 300$–370 K shown in Fig. 6 (left), we obtained ρ_c as a function of T shown in Fig. 6 (right). This result can be fitted by the field emission (FE) model and the thermionic field emission (TFE) model,[43] the former giving $N_D \simeq 3.4 \times 10^{19}$ cm^{-3} and $\Phi_B \simeq 0.42$ eV, and the latter giving $N_D \simeq 1.4 \times 10^{19}$ cm^{-3} and $\Phi_B \simeq 0.42$ eV. We can confirm that the obtained N_D and Φ_B satisfy the criterion for the FE model but do not satisfy that for the TFE model:[44,45] $k_B T < 2E_{00}/[\ln(4\Phi_B/E_F) + (2E_{00}/E_F)^{1/2}]$ for the FE and $k_B T > 2E_{00}/\ln(4\Phi_B/E_F)$ for the TFE using $E_{00} = q\hbar\sqrt{N_D/m^*\varepsilon_s}/2$ with usual notations. Thus, we conclude that the Ohmic contact is dominated by the FE mechanism. The obtained N_D and Φ_B can be used to examine the band diagram for (C).

In Fig. 7, we show the band diagrams obtained by Poisson–Schrödinger calculations for all the cases, (A), (B), (C), and (D). In the case of (A), (B), and (D), the effective barrier heights Φ_B are determined to reproduce the measured n_s. For the case (C), the above-obtained N_D and Φ_B are used. We assume a doping density $N(z) = (N_D - N_{dd})\exp(-z/\xi) + N_{dd}$ (cm^{-3}), where z is the distance from the surface, and ξ is the characteristic length. The first term represents an exponentially decaying polarization doping density according to an exponentially decaying strain.[46] If we set $\xi = 3$ nm, the measured n_s for (C) can be reproduced. The

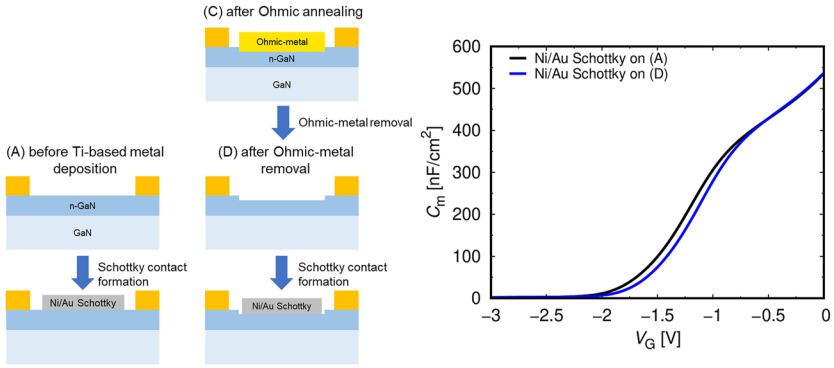

FIG. 5. (Left) The fabrication process of Ni/Au Schottky diodes on the *n*-GaN for (A) and (D). (Right) The capacitance-voltage characteristics of the Ni/Au Schottky diodes.

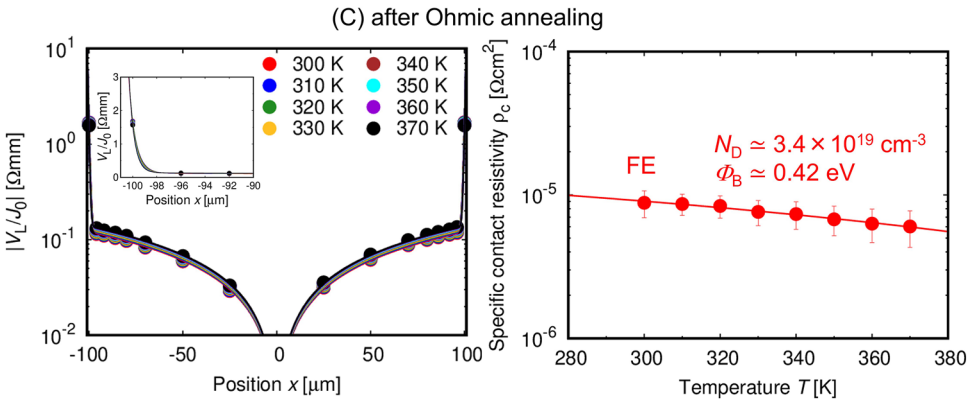

FIG. 6. (Left) The measured $V_L(x)/J_0$ at 300–370 K for (C), with the fitting curves. The inset of the left: the measured $V_L(x)/J_0$ in a linear scale around $x = -100$ μm. (Right) The specific contact resistivity ρ_c as a function of the temperature T for (C), with the FE fitting curve.

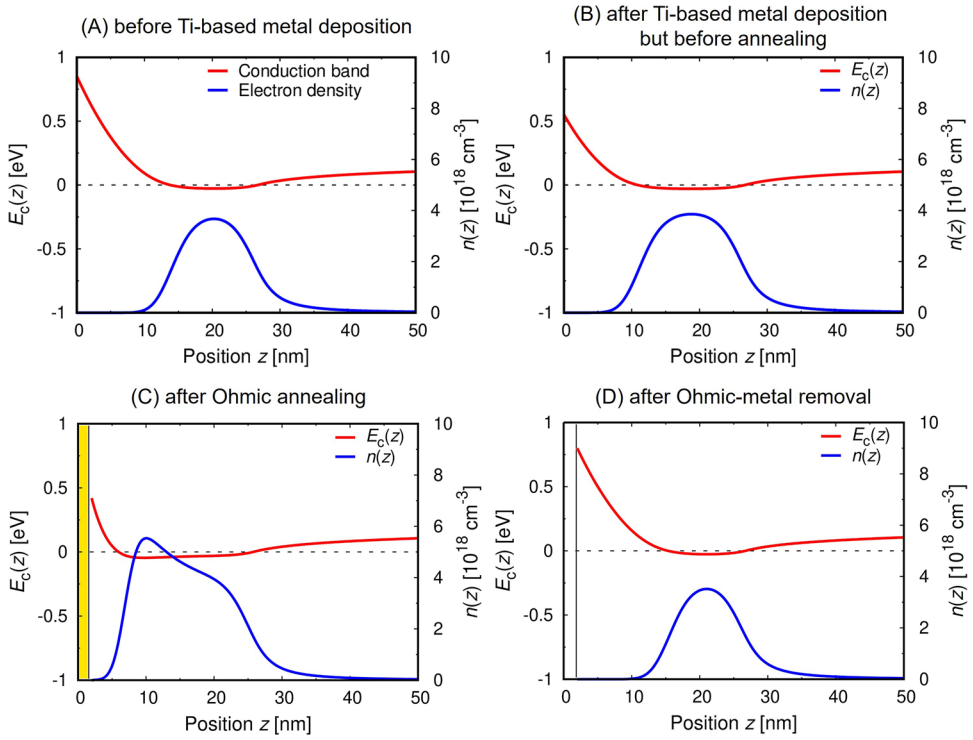

FIG. 7. The calculated conduction bands $E_c(z)$ (red curves) and the local electron densities $n(z)$ (blue curves) for (A)–(D).

obtained conduction bands $E_c(z)$ are shown by the red curves in Fig. 7. We also obtained the local electron densities $n(z)$ (cm^{-3}) shown by the blue curves. The yellow region in (C) illustrates the altered layer. Table I shows a summary of the sheet electron concentration n_s, the electron mobility μ_s, the effective barrier height Φ_B, and the depletion length, for (A), (B), (C), and (D). Owing to the polarization doping near the surface in (C), the depletion length decreases to $\simeq 4$ nm, leading to the Ohmic contact dominated by the FE mechanism. Simultaneously, the electron mobility μ_s for (C) is enhanced. In order to clarify the mechanism, we calculated the local electron mobility $\mu(z) = (1/\mu_{II}(z) + 1/\mu_{po})^{-1}$, using ionized impurity scattering mobility[47]

$$\mu_{II}(z) = \frac{3\varepsilon_s^2 h^3 n(z)}{q^3 m^{*2} N_{dd}} \left[\ln(1+\beta) - \frac{\beta}{1+\beta}\right]^{-1}, \qquad \beta = \frac{4\pi^2 \varepsilon_s \hbar^2}{q^2 m^*} (3\pi^2 n(z))^{1/3}, \tag{3}$$

TABLE I. Summary of the sheet electron concentration n_s, the electron mobility μ_s, the effective barrier height Φ_B, and the depletion length.

	n_s (10^{12} cm^{-2})	μ_s (cm^2/V-s)	Φ_B (eV)	Depletion length (nm)
(A)	4.4	250	0.85	15
(B)	5.7	240	0.55	12
(C)	8.0	320	0.42	4
(D)	3.9	260	0.80	14

and polar optical phonon scattering mobility $\mu_{po} \simeq 3000$ cm^2/V-s evaluated based on Fröhlich interaction.[48] In Fig. 8, the calculated $\mu(z)$ for (B) and (C) are shown by the green dashed-curves. Using these local properties, we obtained the total mobilities,[49–53]

$$\mu_s = \frac{\int n(z)\mu(z)^2 dz}{\int n(z)\mu(z) dz}, \tag{4}$$

which are shown by the green lines in Fig. 8, giving $\mu_s \simeq 240$ cm^2/V-s for (B), and $\mu_s \simeq 300$ cm^2/V-s for (C). They are consistent with the measured $\mu_s \simeq 240$ cm^2/V-s for (B) and $\mu_s \simeq 320 \pm 40$ cm^2/V-s for (C). This indicates that the increase in the electron density by polarization doping leads to the suppression of ionized impurity scattering and consequently the electron mobility enhancement.

In summary, using multi-probe-Hall devices, we investigated the electron transport properties of n-GaN under an Ohmic-metal. We compared the Hall measurement results for n-GaN before Ti-based metal deposition, after Ti-based metal deposition but before annealing, after Ohmic annealing, and after Ohmic-metal removal. We find that, under the Ohmic-metal, n_s is increased and μ_s is enhanced in comparison with those for the other cases. The increased n_s indicates that high-density doping takes place in the n-GaN by the Ohmic annealing, while the high-density doping is not observed after the removal. We conclude that, under the Ohmic-metal, high-density donors are not formed, and high-density polarization doping owing to strain from the Ohmic-metal takes place. In Ref. 19, the role of polarization doping was shown for

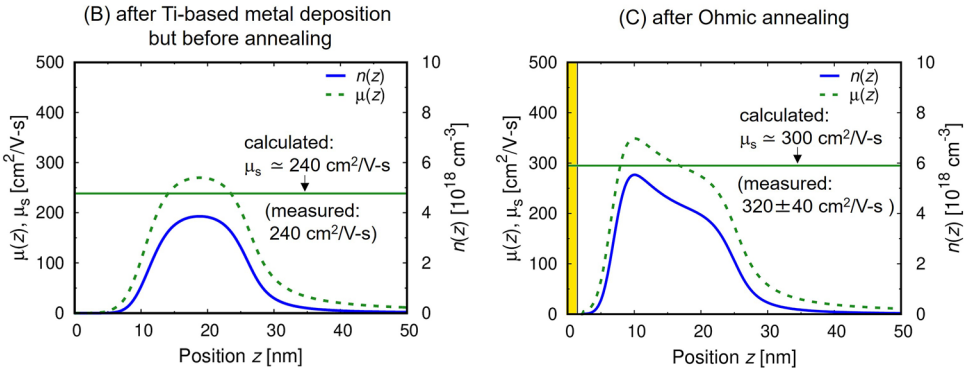

FIG. 8. The calculated local electron mobilities $\mu(z)$ (green dashed-curves) and the total mobilities μ_s (green lines) with the local electron densities $n(z)$ (blue curves) for (B) and (C).

low-temperature ($\lesssim 600\,^{\circ}$C) annealed Ta-based Ohmic-metals contacting to two-dimensional electron gases (2DEGs) in AlGaN/GaN heterostructures. In this work, for low-temperature ($\lesssim 600\,^{\circ}$C) annealed Ti-based Ohmic-metals contacting to three-dimensional electron gases (3DEGs) in *n*-GaN, we elucidate the role of polarization doping and find the electron mobility enhancement owing to the suppression of ionized impurity scattering through an increase in electron density without donors. While metal penetration into the semiconductor is important for high-temperature ($\geq 800\,^{\circ}$C) annealed Ohmic contacts to nitride semiconductors,[40] we conclude that polarization doping is essential for low-temperature annealed Ohmic contacts. On the other hand, this work shows that the ~ 2-nm altered layer for the low-temperature annealed Ti-based Ohmic-metals is etched by an acidic solution, while such etching was not observed for the low-temperature annealed Ta-based Ohmic-metals.[19] This suggests that there are different aspects between the Ti- and Ta-based Ohmic-metals, even though polarization doping plays an important role for both the Ohmic-metals.

This work was supported by the JSPS KAKENHI under Grant No. JP22H01545.

AUTHOR DECLARATIONS

Conflict of Interest

The authors have no conflicts to disclose.

Author Contributions

Kazuya Uryu: Data curation (lead); Formal analysis (lead); Investigation (lead); Methodology (equal); Writing – original draft (lead). **Yuchen Deng**: Data curation (supporting); Investigation (supporting); Writing – review & editing (supporting). **Son Phuong Le**: Resources (lead); Writing – review & editing (supporting). **Toshikazu Suzuki**: Conceptualization (lead); Funding acquisition (lead); Methodology (equal); Project administration (lead); Supervision (lead); Writing – review & editing (lead).

DATA AVAILABILITY

The data that support the findings of this study are available from the corresponding author upon reasonable request.

REFERENCES

[1] D. K. Schroder, *Semiconductor Material and Device Characterization* (John Wiley & Sons, Ltd, 2005), p. 147.
[2] H. Morkoç, *Handbook of Nitride Semiconductors and Devices, Electronic and Optical Processes in Nitrides* (John Wiley & Sons, Ltd, 2008), p. 41.
[3] H. H. Berger, Solid State Electron. **15**, 145 (1972).
[4] G. K. Reeves and H. B. Harrison, IEEE Electron Device Lett. **3**, 111 (1982).
[5] H. P. Kattelus, J. L. Tandon, and M.-A. Nicolet, Solid State Electron. **29**, 903 (1986).
[6] H. G. Henry, IEEE Trans. Electron Devices **36**, 1390 (1989).
[7] M. Ahmad, A. P. Shah, D. K. Sharma, N. R. Roy, and B. M. Arora, Solid State Electron. **46**, 505 (2002).
[8] Y. Sun, X. Chen, and L. F. Eastman, J. Appl. Phys. **98**, 053701 (2005).
[9] M. Hajłasz, J. J. T. M. Donkers, S. J. Sque, S. B. S. Heil, D. J. Gravesteijn, F. J. R. Rietveld, and J. Schmitz, Appl. Phys. Lett. **104**, 242109 (2014).
[10] M. Hajłasz, J. J. T. M. Donkers, S. J. Sque, S. B. S. Heil, D. J. Gravesteijn, F. J. R. Rietveld, and J. Schmitz, in *Proceedings of the 2015 International Conference on Microelectronic Test Structures* (IEEE, 2015), pp. 158–162.
[11] M. Spera, C. Miccoli, R. L. Nigro, C. Bongiorno, D. Corso, S. Di Franco, F. Iucolano, F. Roccaforte, and G. Greco, Mater. Sci. Semicond. Process. **78**, 111 (2018).
[12] S. Venica, F. Driussi, A. Gahoi, P. Palestri, M. C. Lemme, and L. Selmi, IEEE Trans. Electron Devices **65**, 1589 (2018).
[13] M. König, G. Ruhl, A. Gahoi, S. Wittmann, T. Preis, J.-M. Batke, I. Costina, and M. C. Lemme, IEEE J. Electron Devices Soc. **7**, 219 (2019).
[14] L. P. Floyd, T. Scheuermann, P. A. F. Herbert, and W. M. Kelly, Solid State Electron. **37**, 1579 (1994).
[15] D. Sawdai, D. Pavlidis, and D. Cui, IEEE Trans. Electron Devices **46**, 1302 (1999).
[16] M. Lijadi, F. Pardo, N. Bardou, and J.-L. Pelouard, Solid State Electron. **49**, 1655 (2005).
[17] K. Uryu, S. Kiuchi, and T. Suzuki, Appl. Phys. Lett. **119**, 023505 (2021).
[18] D. Jena, S. Heikman, D. Green, D. Buttari, R. Coffie, H. Xing, S. Keller, S. DenBaars, J. S. Speck, U. K. Mishra, and I. Smorchkova, Appl. Phys. Lett. **81**, 4395 (2002).
[19] K. Uryu, S. Kiuchi, T. Sato, and T. Suzuki, Appl. Phys. Lett. **120**, 052104 (2022).

[20] A. Malmros, H. Blanck, and N. Rorsman, Semicond. Sci. Technol. **26**, 075006 (2011).
[21] B. P. Luther, S. E. Mohney, T. N. Jackson, M. Asif Khan, Q. Chen, and J. W. Yang, Appl. Phys. Lett. **70**, 57 (1997).
[22] J. D. Hwang, G. H. Yang, W. T. Chang, C. C. Lin, R. W. Chuang, and S. J. Chang, Microelectron. Eng. **77**, 71 (2005).
[23] M.-L. Lee, J.-K. Sheu, and C. C. Hu, Appl. Phys. Lett. **91**, 182106 (2007).
[24] R. France, T. Xu, P. Chen, R. Chandrasekaran, and T. D. Moustakas, Appl. Phys. Lett. **90**, 062115 (2007).
[25] G. Greco, F. Iucolano, and F. Roccaforte, Appl. Surf. Sci. **383**, 324 (2016).
[26] M. E. Lin, Z. Ma, F. Y. Huang, Z. F. Fan, L. H. Allen, and H. Morkoç, Appl. Phys. Lett. **64**, 1003 (1994).
[27] J. D. Guo, C. I. Lin, M. S. Feng, F. M. Pan, G. C. Chi, and C. T. Lee, Appl. Phys. Lett. **68**, 235 (1996).
[28] C. Lu, H. Chen, X. Lv, X. Xie, and S. N. Mohammad, J. Appl. Phys. **91**, 9218 (2002).
[29] V. Kumar, L. Zhou, D. Selvanathan, and I. Adesida, J. Appl. Phys. **92**, 1712 (2002).
[30] A. Motayed, R. Bathe, M. C. Wood, O. S. Diouf, R. D. Vispute, and S. N. Mohammad, J. Appl. Phys. **93**, 1087 (2003).
[31] A. Motayed, K. A. Jones, M. A. Derenge, M. C. Wood, D. N. Zakharov, Z. Liliental-Weber, D. J. Smith, A. V. Davydov, W. T. Anderson, A. A. Iliadis, and S. Noor Mohammad, J. Appl. Phys. **95**, 1516 (2004).
[32] L. Wang, F. M. Mohammed, and I. Adesida, J. Appl. Phys. **98**, 106105 (2005).
[33] W. Hou, T. Detchprohm, and C. Wetzel, Appl. Phys. Lett. **101**, 242105 (2012).
[34] S. Ruvimov, Z. Liliental-Weber, J. Washburn, K. J. Duxstad, E. E. Haller, Z. F. Fan, S. N. Mohammad, W. Kim, A. E. Botchkarev, and H. Morkoç, Appl. Phys. Lett. **69**, 1556 (1996).
[35] F. Iucolano, F. Roccaforte, A. Alberti, C. Bongiorno, S. Di Franco, and V. Raineri, J. Appl. Phys. **100**, 123706 (2006).
[36] A. Shriki, R. Winter, Y. Calahorra, Y. Kauffmann, G. Ankonina, M. Eizenberg, and D. Ritter, J. Appl. Phys. **121**, 065301 (2017).
[37] A. Kakanakova-Georgieva, U. Forsberg, I. G. Ivanov, and E. Janzén, J. Cryst. Growth **300**, 100 (2007).
[38] C. J. Lu, A. V. Davydov, D. Josell, and L. A. Bendersky, J. Appl. Phys. **94**, 245 (2003).
[39] B. Van Daele, G. Van Tendeloo, W. Ruythooren, J. Derluyn, M. R. Leys, and M. Germain, Appl. Phys. Lett. **87**, 061905 (2005).
[40] L. Wang, F. M. Mohammed, and I. Adesida, J. Appl. Phys. **101**, 013702 (2007).
[41] S. Rajan, S. P. DenBaars, U. K. Mishra, H. Xing, and D. Jena, Appl. Phys. Lett. **88**, 042103 (2006).
[42] M. Zhu, M. Qi, K. Nomoto, Z. Hu, B. Song, M. Pan, X. Gao, D. Jena, and H. G. Xing, Appl. Phys. Lett. **110**, 182102 (2017).
[43] A. Y. C. Yu, Solid State Electron. **13**, 239 (1970).
[44] E. L. Murphy and R. H. Good, Phys. Rev. **102**, 1464 (1956).
[45] F. A. Padovani and R. Stratton, Solid State Electron. **9**, 695 (1966).
[46] M. Murakami and R. W. Vook, Crit. Rev. Solid State Mater. Sci. **11**, 317 (1983).
[47] I. Halidou, Z. Benzarti, Z. Chine, T. Boufaden, and B. El Jani, Microelectron. J. **32**, 137 (2001).
[48] C. Hamaguchi, *Basic Semiconductor Physics* (Springer International Publishing, 2017), p. 351.
[49] R. L. Petritz, Phys. Rev. **110**, 1254 (1958).
[50] G. Ghibaudo and G. Kamarinos, Rev. Phys. Appl. **17**, 133 (1982).
[51] G. Ghibaudo, J. Phys. C: Solid State Phys. **19**, 767 (1986).
[52] S. B. Lisesivdin, N. Balkan, and E. Ozbay, Microelectron. J. **40**, 413 (2009).
[53] M. A. Negara, D. Veksler, J. Huang, G. Ghibaudo, P. K. Hurley, G. Bersuker, N. Goel, and P. Kirsch, Appl. Phys. Lett. **99**, 232101 (2011).